Relativistic breather-type solitary waves with linear polarization in cold plasmas

G. Sánchez-Arriaga,[1] E. Siminos,[2] V. Saxena,[3] and I. Kourakis[4]

[1]*Departamento de Física Aplicada, Escuela Técnica Superior de Ingenieros Aeronáuticos, Universidad Politécnica de Madrid, Madrid, Spain*

[2]*Max Planck Institute for the Physics of Complex Systems, Nöthnitzer Str. 38, D-01187 Dresden, Germany*

[3]*Centre for Free-Electron Laser Science, Deutsches Elektronen-Synchrotron, Notkestrasse 85, 22607 Hamburg, Germany*

[4]*Centre for Plasma Physics, School of Mathematics and Physics, Queen's University Belfast, Belfast BT7 1NN,*

Northern Ireland, United Kingdom

Linearly polarized solitary waves, arising from the interaction of an intense laser pulse with a plasma, are investigated. Localized structures, in the form of exact numerical nonlinear solutions of the one-dimensional Maxwell-fluid model for a cold plasma with fixed ions, are presented. Unlike stationary circularly polarized solitary waves, the linear polarization gives rise to a breather-type behavior and a periodic exchange of electromagnetic energy and electron kinetic energy at twice the frequency of the wave. A numerical method based on a finite-differences scheme allows us to compute a branch of solutions within the frequency range $\Omega_{\min} < \Omega < \omega_{pe}$, where ω_{pe} and $\Omega_{\min}$ are the electron plasma frequency and the frequency value for which the plasma density vanishes locally, respectively. A detailed description of the spatiotemporal structure of the waves and their main properties as a function of Ω is presented. Small-amplitude oscillations appearing in the tail of the solitary waves, a consequence of the linear polarization and harmonic excitation, are explained with the aid of the Akhiezer-Polovin system. Direct numerical simulations of the Maxwell-fluid model show that these solitary waves propagate without change for a long time.

I. INTRODUCTION

Electromagnetic relativistic solitary waves, commonly named relativistic solitons, are self-trapped localized structures that are excited during the interaction of a high-intensity laser with a plasma. They typically consist on a region of rarified plasma where a high-amplitude electromagnetic wave, with frequency below the laser frequency, is trapped. A solitary wave can be classified according to its polarization (linear or circular), its group velocity (standing or moving waves), and its state (isolated structure or embedded in long laser pulses). Since part of the laser energy is dedicated to exciting them, they may affect certain laser applications like inertial confinement fusion, particle acceleration, plasma lens for ultraintense laser focusing, and high-brightness x- and gamma ray generation [1]. They also offer an excellent opportunity to confront theoretical and experimental works and enhance our knowledge of nonlinear waves in plasmas.

This great variety of solitary waves has been the subject of important research activity in plasma physics, including analytical work, numerical simulations, and laboratory experiments. Pioneer works [2–4] were followed by intense activity mainly in the framework of the relativistic fluid model. Exact one-dimensional (1D) circularly polarized solitary wave solutions, including isolated [5–7] and embedded in long laser pulses [7–9] waves, were found. Single-hump and multihump solitons are possible. All these solutions, except the one presented in Ref. [5] that admits an analytical form, were found numerically. The analysis of linearly polarized waves, however, is more difficult mainly due to the high harmonic generation. Some approximate 1D solutions have been presented in the weak-amplitude limit [10,11] and in the framework of the Akhiezer-Polovin system [12]. Exact two-dimensional (2D) linearly polarized solitary wave solutions

of the fluid model were also found [13]. Solitary waves were observed in particle-in-cell (PIC) codes [14–16], and their footprints were detected in laboratory experiments [17–21].

In theoretical works, analysis was mostly focused on the spatiotemporal structures of the plasma and electromagnetic fields and the relationship between the amplitude of the electromagnetic wave and its frequency. A central role in the analysis was also played by the organization of the solitons in parameter space, i.e., in the velocity and frequency plane. Some solitary waves are organized in branches: given a value of the group velocity, the soliton exists for a single frequency value. Examples of this type are the circularly polarized moving solitons discovered in Ref. [6]. On the other hand, other types of solitons, like the circularly polarized standing soliton found in Ref. [5] or the embedded solitons of Refs. [8] and [9], have a *continuous spectrum*. In this case, for a given velocity, solitons exist for any frequency within a certain range. The discrete or continuous character of the spectrum can be anticipated by using arguments from dynamical system theory, including the dimension of the system, the characteristics of the stable and unstable manifolds of fixed points and the Hamiltonian and/or reversible character of the system [8].

A common feature to all the previously cited 1D solitons is the stationary character of the soliton profile in a frame moving with its group velocity. Under the traveling wave ansatz, the amplitude of the solutions just depends on the coordinate $\xi = x - Vt$. However, in recent fluid simulations aimed at the interaction of an ultrashort laser pulse with an overdense plasma in the relativistic transparency regime, solitonic structures with a breather-like behavior were observed [22]. Energy exchange between the soliton and the plasma occurred at twice the laser frequency. These periodic oscillations in time of the soliton amplitude is a less known aspect in 1D fluid theory but

a well-known feature for linearly *s*-polarized 2D solitons, as shown by past PIC simulation [15] and more recent solutions found in the fluid model [8]. An oscillatory behavior of 1D linearly polarized solitary waves was also observed in PIC simulations of laser-plasma interactions [23].

These observations in both fluid [22] and PIC simulations [23] motivate us to determine numerically exact linearly polarized solitary wave solutions of the relativistic fluid model. Following the findings of Ref. [22], we did not restrict the analysis to stationary solutions, but let them oscillate periodically in time. From a numerical point of view, this a challenging problem because one needs to work with a system of partial differential equations (instead of ordinary differential equations). This method, unlike the excitation of solitary waves with laser pulses in fluid or PIC simulations, provides the frequency-amplitude relation and the frequency range of existence of the waves. Section II introduces the relevant equations of the model and presents the numerical method used to compute the solitary waves. Results on standing solitary waves are presented in Sec. III, including their spatiotemporal structure, a simple analysis based on energy conservation, and the dependence of their main properties as a function of the frequency. The stability is explored in Sec. IV with the aid of full nonstationary fluid simulations. Our conclusions are summarized in Sec. V.

II. PHYSICAL AND NUMERICAL MODEL

A. The relativistic fluid model

We consider a plasma consisting of electrons and immobile ions. For convenience, length, time, velocity, momentum, vector and scalar potentials, and density are normalized over c/ω_{pe}, ω_{pe}^{-1}, c, $m_e c$, $m_e c^2/e$, and n_0, respectively. Here n_0, $\omega_{pe} = \sqrt{4\pi n_0 e^2/m_e}$, m_e, and c are the unperturbed plasma density, the electron plasma frequency, the electron mass, and the speed of light. The Maxwell (in the Coulomb gauge) and plasma equations then read

$$\Delta \mathbf{A} - \frac{\partial^2 \mathbf{A}}{\partial t^2} - \frac{\partial}{\partial t}\nabla\phi = n\mathbf{v}, \qquad (1a)$$

$$\Delta\phi = n - 1, \qquad (1b)$$

$$\frac{\partial n}{\partial t} + \nabla \cdot (n\mathbf{v}) = 0, \qquad (1c)$$

$$\frac{\partial \mathbf{P}}{\partial t} - \mathbf{v} \times (\nabla \times \mathbf{P}) = \nabla(\phi - \gamma), \qquad (1d)$$

where $\mathbf{A}$ and ϕ are the vector and scalar potentials, $\mathbf{P} = \mathbf{p} - \mathbf{A}$, $\gamma = \sqrt{1 + |\mathbf{p}|^2}$, and $\mathbf{p}$ and $\mathbf{v} = \mathbf{p}/\gamma$ are the electron momentum and velocity, respectively. In this model the plasma is assumed to be cold since the typical background thermal velocities are much smaller than the relativistic quiver velocity of electrons in the strong electromagnetic field. Extensions of previous works on relativistic solitons to include a finite temperature have shown that certain features of the solitons change, but that the cold fluid model remains a useful first approximation [8,24].

Here we restrict the analysis to 1D waves ($\partial_y = \partial_z = 0$) propagating along the x direction. Coulomb gauge and the transverse components of Eq. (1d) give $A_x = 0$ and $P_y =$

$P_z = 0$, respectively. Using these results in Eqs. (1a)–(1d), one finds

$$\frac{\partial^2 \phi}{\partial t \partial x} + \frac{n}{\gamma} p_x = 0, \qquad (2a)$$

$$\frac{\partial A_{y,z}}{\partial x^2} - \frac{\partial^2 A_{y,z}}{\partial t^2} - \frac{n}{\gamma} A_{y,z} = 0, \qquad (2b)$$

$$n = 1 + \frac{\partial^2 \phi}{\partial x^2}, \qquad (2c)$$

$$\frac{\partial n}{\partial t} + \frac{\partial}{\partial x}\left(\frac{n p_x}{\gamma}\right) = 0, \qquad (2d)$$

$$\frac{\partial p_x}{\partial t} = \frac{\partial}{\partial x}(\phi - \gamma). \qquad (2e)$$

B. The Akhiezer-Polovin system

Before we discuss solitary wave solutions of Eqs. (2a)–(2e), we first review some concepts of the Akhiezer-Polovin set of equations [2]. This system, which is a subset of Eqs. (2a)–(2e), is obtained by assuming that all the variables depend on the coordinate $\xi = x - Vt$, with $V \equiv \omega/k > 1$ the normalized phase velocity. The result is a set of two ordinary differential equations that are simpler than Eqs. (2a)–(2e). The purpose of this short analysis is twofold. On one hand, analytical tools from the theory of dynamical systems show that linearly polarized and isolated solitary waves depending only on ξ are not possible. This property suggests that one may look for solitary waves depending separately on x and t. This procedure is followed in Sec. III. On the other hand, the dispersion relation of the Akhiezer-Polovin system will help us to understand the results of Sec. III concerning small-amplitude oscillations at the tail of the solitary wave.

Taking linear polarization, $\mathbf{A} = a(\xi)\mathbf{u}_y$, Eqs. (2a)–(2e) become

$$\frac{d}{d\xi}\left[-Vn + n\frac{p_x}{\gamma}\right] = 0 \rightarrow -Vn + n\frac{p_x}{\gamma} = -V, \quad (3a)$$

$$\frac{d}{d\xi}[V p_x + \phi - \gamma] = 0 \rightarrow V p_x + \phi - \gamma = -\Gamma, \quad (3b)$$

$$\frac{d^2\phi}{d\xi^2} = n - 1, \qquad (3c)$$

$$(V^2 - 1)\frac{d^2 a}{d\xi^2} + \frac{n}{\gamma}a = 0, \qquad (3d)$$

where we assumed that at a certain position, ξ_0, one has

$$a(\xi_0) = a_0, \quad \phi(\xi_0) = 0, \quad p_x(\xi_0) = 0, \quad n(\xi_0) = 1, \quad (4)$$

and we introduced the constant $\Gamma \equiv \sqrt{1 + a_0^2}$. Defining $\psi \equiv \Gamma + \phi$ and $R \equiv \sqrt{\psi^2 - (1 - V^2)(1 + a^2)}$, Eqs. (3a), (3b), and $\gamma = \sqrt{1 + a^2 + p_x^2}$ give $p_x = (V\psi - R)/(1 - V^2)$, $n = V(\psi - VR)/R(1 - V^2)$, and $\gamma = (\psi - VR)/(1 - V^2)$. The substitution of these results in Eqs. (3c) and (3d) yields [2,25]

$$\frac{d^2 a}{d\xi^2} = -\frac{V}{V^2 - 1}\frac{a}{R}, \qquad (5a)$$

$$\frac{d^2\phi}{d\xi^2} = -\frac{V}{V^2 - 1}\left(\frac{\psi}{R} - \frac{1}{V}\right). \qquad (5b)$$

The above system can be written in Hamiltonian form. The Hamiltonian function

$$H = \frac{1}{2}\left(V^2 - 1\right)\dot{a}^2 + \frac{1}{2}\dot{\phi}^2 + \frac{V}{V^2 - 1}(R - V) - \frac{\phi}{V^2 - 1},$$
(6)

which does not depend explicitly on ξ, is a constant of motion. In the small but finite amplitude limit with low-density plasma $(V \to 1)$, Eq. (5) shows that the dispersion relation (in physical units) for the transverse oscillations is given by [2]

$$\omega \approx kc + \frac{\omega_{pe}^2}{2kc}\left(1 - \frac{a_0^2}{2}\right).$$
(7)

Higher order corrections can be found in Ref. [26]. The longitudinal variable, ϕ, oscillates with frequency 2ω and an amplitude of the order of a_0^2.

Equations (5) can be written as $d\mathbf{y}/d\xi = \mathbf{f}(\mathbf{y})$, and arguments from the theory of dynamical systems can be used to discuss the existence of solitary waves [27]. We introduce the notion of the stable (unstable) manifold W^s (W^i) of an invariant set $\mathcal{M}$, as the set of forward (backward) in ξ trajectories that terminate at $\mathcal{M}$. The invariant set of interest here are the equilibrium points $\mathbf{y}^*$ and the periodic orbits $\mathbf{y}_p$, that satisfy $\mathbf{f}(\mathbf{y}^*) = 0$, and $\mathbf{y}_p(t) = \mathbf{y}_p(t + T)$, respectively. Since solitary waves are homoclinic orbits, i.e., they approach $\mathcal{M}$ as $\xi \to \pm\infty$, they lie in the intersection of W^s and W^i. A local analysis of the stability of $\mathbf{y}^*$ or $\mathbf{y}_p$ can help to decide the existence of solitary waves. For example, if there is no W^s and W^i because the equilibrium point is a center, then homoclinic orbits cannot exist.

If $a_0 \neq 0$, then the phase space point $(a,\dot{a},\phi,\dot{\phi}) = (a_0,0,0,0) \equiv Q_0$ is not an equilibrium state of Eqs. (5); solitary waves with $a \to a_0$ as $\xi \to \pm\infty$ are not possible. On the other hand, if $a_0 = 0$, then Q_0 is an equilibrium state, and one may try to look for solitary waves, i.e., homoclinic orbits connecting to Q_0 at $\xi \to \pm\infty$. However, orbits cannot connect to Q_0 because a standard stability analysis of Q_0 shows that it is a center with eigenvalues $\lambda_{1,2} = \pm i\sqrt{1/(V^2 - 1)}$ and $\lambda_{3,4} = \pm i/V$. By going back to physical units, one verifies that "frequency" $1/V$ corresponds to longitudinal oscillations at the plasma frequency ω_{pe}. The "frequency" $\sqrt{1/(V^2 - 1)}$ corresponds to linear electromagnetic waves, and it reduces to Eq. (7) in the small-amplitude and low plasma density limit.

The above discussion rules out the existence of homoclinic orbits to Q_0. From a physical point of view they would represent isolated solitary waves, with linear polarization, and stationary in a frame of reference moving with V. However, as previously discussed, one could also try to look for homoclinic orbits connecting to a periodic solution as $\xi \to \pm\infty$. These structures, which were constructed using Poincaré analysis in Ref. [12], are solitary waves embedded in long laser pulses. We remark that, since we used Eq. (4) to derive Eqs. (5), only orbits of Sys. (5) passing through the surface $(a,\dot{a},\phi,\dot{\phi}) = (a_0,\dot{a},0,\dot{\phi})$ are relevant from a physical point of view. Other orbits would be a solution of Eqs. (5) but not of the fluid model [Eq. (1)].

C. Locating generalized solitary waves

A new class of solitary waves is found if we let the solutions vary with time in the ξ frame. Physically, such a broader model is necessary to take into account the appearance of new frequencies in the solution. It requires a more general mathematical framework than the Akhiezer-Polovin system. For this purpose, scaled spatial and temporal variables $X = x/L$ and $\tau = t/T$ are introduced, with T and L the temporal and spatial periods of the solution. Equations (2a)–(2e) then read

$$\frac{1}{L^2}\frac{\partial^2 A_{y,z}}{\partial X^2} - \frac{1}{T^2}\frac{\partial^2 A_{y,z}}{\partial \tau^2} - \frac{n}{\gamma}A_{y,z} = 0,$$
(8a)

$$\frac{1}{T^2}\frac{\partial^2 p_x}{\partial \tau^2} + \frac{1}{TL}\frac{\partial^2 \gamma}{\partial X \partial \tau} + \frac{n}{\gamma}p_x = 0,$$
(8b)

with

$$n = 1 + \frac{1}{TL}\frac{\partial^2 p_x}{\partial X \partial \tau} + \frac{1}{L^2}\frac{\partial^2 \gamma}{\partial X^2},$$
(9a)

$$\gamma = \sqrt{1 + p_x^2 + A_y^2 + A_z^2},$$
(9b)

and Eq. (2e) was used to eliminate ϕ. We remark that T and L appear now as free parameters in Eqs. (8). For convenience, the solitary wave frequency $\Omega = 2\pi/T$ (instead of T) will be used as a bifurcation parameter to present our results. As explained below, L is found with the aid of a phase condition for each Ω value.

Our algorithm solves Eqs. (8) as follows. The computational box $(0 < X < 1) \times (0 < \tau < 1)$ is discretized with $N_x \times N_\tau$ uniformly distributed points. Here N_x and N_τ are integer numbers. A state vector $\mathbf{x}_s = [A_y\ A_z\ p_x\ L]$ of dimension $3 \times N_x \times N_\tau + 1$ is constructed. It contains the unknowns of the problem, i.e., the values of A_y, A_z, and p_x at the grid points and the length of the computational domain. Differential operators in Eqs. (8) are substituted by second order finite difference formulas. At the border of the box one may take into account the boundary conditions of the problem. Here we are interested in periodic in time solutions $A_{y,z}(X,\tau + T) = A_{y,z}(X,\tau)$ and $p_x(X,\tau + T) = p_x(X,\tau)$ and two types of spatial boundary conditions: (i) vanishing $A_{y,z}(0,\tau) = A_{y,z}(L,\tau) = p_x(0,\tau) = p_x(L,\tau) = 0$ and (ii) periodic $A_{y,z}(X,\tau) = A_{y,z}(X + L,\tau)$ and $p_x(X,\tau) = p_x(X + L,\tau)$. The use of finite differences transforms Eqs. (8) into a system of $3N_x \times N_\tau$ nonlinear algebraic equations.

The algorithm is closed by taking into account that the problem is invariant under temporal and spatial translations. Its solution is not unique, but rather is a continuous family. In order to remove this arbitrary *phase variable* and restrict the solution to a unique member of the family, a *phase condition* was added. We found that

$$\left.\frac{\partial^2 A_y}{\partial X \partial \tau}\right|_{X=0.5,\tau=0.5} = 0$$
(10)

serves this purpose and allows the code to converge to the solution in few iterations. Equation (10) was also approximated by the corresponding finite-difference formula.

The set of $3N_x \times N_\tau + 1$ algebraic equations,
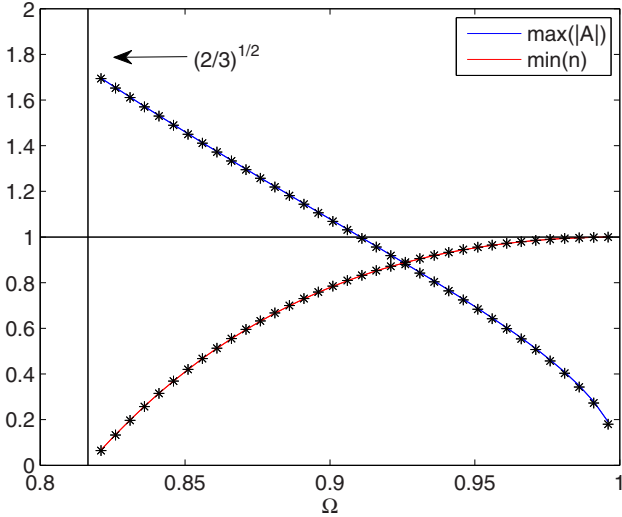
$$\mathbf{F}(\mathbf{x}_s) = 0,$$
(11)

FIG. 1. (Color online) Maximum amplitude, $max(|A|)$, and minimum density, $min(n)$, for circularly polarized solitary waves. All variables are normalized (see Sec. II). Circles (solid lines) correspond to solutions computed with our numerical code (analytical solution given in Ref. [5]).
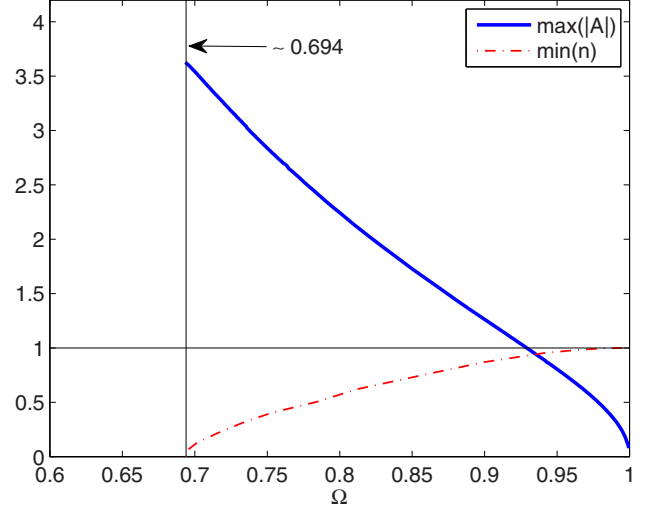

FIG. 2. (Color online) Maximum amplitude (solid blue line) and minimum density (dashed red line) values versus the normalized frequency for linearly polarized solitary waves.

was solved with a Newton-Raphson method. The speed of the algorithm was enhanced by computing analytically the Jacobian, $\bar{J}$, of $F(x_s)$ and using parallel computations to find the LU decomposition of $\bar{J}$ for each iteration. The tolerance of our solutions, $Error = max\,[F(x_s)]$, was less than 10^{-8}. The initial guess used to initialize the Newton-Raphson method depends on the solution under consideration, as discussed shortly.

The code was validated with the circularly polarized solitary waves obtained by Esirkepov *et al.* [5]. For these calculations we set $N_x = 1000$ and $N_\tau = 60$. The comparison between the analytical formula given in Ref. [5] and the result of our code is shown in Fig. 1. At each Ω, we used as initial guess for the Newton method the solution obtained at the previous Ω value in the branch. For the first frequency, $\Omega = 0.996$, the analytical formula was used. The calculations were carried out with periodic and vanishing boundary conditions in space. Both schemes yielded the same results, which are in good agreement with the analytical formulas. For this solution one has $|A| \rightarrow 0$ as $\Omega \rightarrow \omega_{pe}$ and the branch extends until $\Omega = \sqrt{2/3}\,\omega_{pe}$, where the minimum density vanishes.

III. BREATHER-LIKE SOLITARY WAVES

A. Branch of solutions

We now focus on linearly polarized solitary waves and set $A_z = 0$ in Eqs. (8a) and (8b). The number of unknowns in Eq. (11) is equal to $2N_x N_\tau + 1$, thus reducing the computational load as compared with the circularly polarized case. The guess to initialize the Newton-Raphson algorithm was taken from Ref. [11], which presented an analytical formula for linearly polarized solitary waves. This solution is not exact but valid only for a frequency close to ω_{pe}, where the amplitude of the wave vanishes. In this limit, the authors derived a nonlinear Schrödinger equation with

local and nonlocal cubic nonlinearities and found a standing electromagnetic solitary wave. Fortunately, this solution is *close* enough to our breather-like wave. Here *close* means that our Newton method started with this wave converges to a solution during the iterative process. Once a breather-like solution is known for a Ω value close to ω_{pe}, the branch of solution is continued by using Ω as a bifurcation parameter. For each parameter value the spatiotemporal structure of the solitary wave was obtained. Typical resolutions in the calculations were $N_x = 1001$ and $N_\tau = 101$, and the length of the computational box dynamically changed during the calculation within the range $100 < L < 200$. To check the integrity of the solutions, the same calculations but with different resolutions were also carried out.

Figure 2 shows the maximum of the vector potential (blue thick line) and the minimum density (dashed red line) values of the solitary waves versus the frequency Ω. The behavior is qualitatively similar to the circularly polarized case (see Fig. 1): (i) solitary waves exist in a frequency range $\Omega_{min} < \Omega < \omega_{pe}$, (ii) $max(|A|) \rightarrow 0$, $min(n) \rightarrow 1$, and the width increases as $\Omega \rightarrow \omega_{pe}$, and (iii) the maximum of the amplitude increases and $min(n) \rightarrow 0$ as the frequency approaches $\Omega_{min} \approx 0.694$. A comparison of Figs. 1 and 2 shows that, for a given frequency, linearly polarized waves have greater amplitude than circularly polarized waves. They also exist in a broader frequency range because $\Omega_{min} = 0.694 < \sqrt{2/3} \approx 0.817$.

B. Spatiotemporal structure of the waves

Figure 3 shows the spatiotemporal evolution of a solitary wave with $\Omega = 0.9\omega_{pe}$. Similarly to circularly polarized solitons, there is a rarified plasma region and an electromagnetic wave oscillating inside [see panels (a) and (c)]. However, linearly polarized waves present two distinguishing features: (i) the plasma cavity has a time modulation [see panel (c)] and (ii) longitudinal electron momentum p_x, electron density, and γ factor oscillate twice as fast as the vector potential.
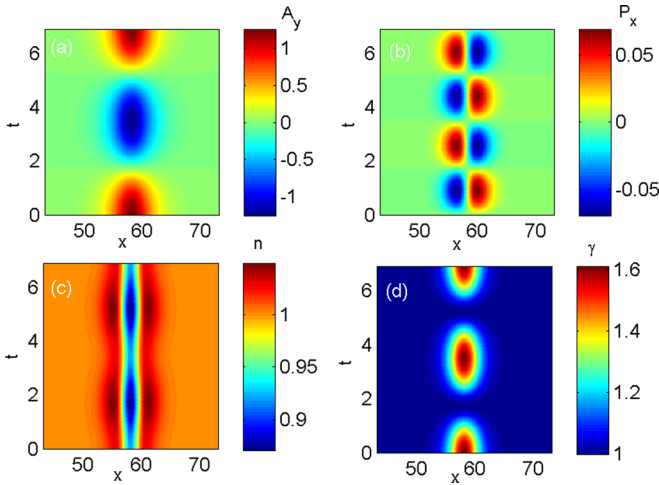
FIG. 3. (Color online) Spatiotemporal evolution of a linearly polarized soliton with $\Omega = 0.9\omega_{pe}$. Numerical values are $N_x = 1001$, $N_\tau = 101$. Panels (a) to (d) show the normalized vector potential component A_y, the longitudinal momentum p_x, and the density n and γ, respectively. The normalization of the variables is explained in Sec. II.

FIG. 4. (Color online) Panels (a) to (d) show the (normalized) electric field components E_y, E_x, the magnetic field component b_z, and the electromagnetic energy density $u = (E_x^2 + E_y^2 + B_z^2)/2$, respectively, for the same parameter values as in Fig. 3.

From Eq. (2e), we observe that electron oscillations come from the actions of the electrostatic force due to the charge separation and the ponderomotive force. The momentum in panel (b) oscillates twice as fast because of the second-harmonic oscillating component of the ponderomotive force. The modulation in time of the plasma cavity is correlated with the behavior of the vector potential: as shown by panels (a) and (c), the lowest plasma density inside the cavity is reached when the electromagnetic wave vanishes.

An analysis of the electromagnetic fields and the electromagnetic energy density ($u = (|\boldsymbol{E}|^2 + |\boldsymbol{B}|^2)/2$) helps to understand the physics of the solitary waves and their connection or generalization to the s-polarized 2D solitary waves studied in Refs. [15] and [13] (see Figs. 4 and 5). In either 1D or 2D geometry, the vector potential and electric field components A_y and E_y oscillate at the frequency of the solitary wave (below the plasma frequency). The electromagnetic wave is trapped inside the cavity. They have electric field components, E_x for 1D and a radial component E_r for 2D waves, which always point outside the solitary wave. These electric field components produce a force that tries to bring the electrons back to the center of the wave, and, unlike E_y, their time variation is very weak [see Fig. 4(b)]. Since $\boldsymbol{p}_y = A_y$, there is a current in the y direction that produces a B_z component and an azimuthal component B_θ for 1D and 2D solitary waves, respectively.

As shown by Fig. 5 one of the main consequences of removing the hypothesis $\partial/\partial z = 0$, and thus changing from a 1D to a 2D configuration, is the confinement of the magnetic field. For 1D waves B_z extends from $z \to -\infty$ to $z \to +\infty$, but for 2D it becomes azimuthal and remains inside the cavity. In a three-dimensional configuration, where the electric field component E_y cannot extend from $y \to -\infty$ to $y \to +\infty$, a change of topology happens in order to confine the full structure inside a bubble. Such a structure has been observed in PIC simulations [16]. However, to the best of our knowledge,
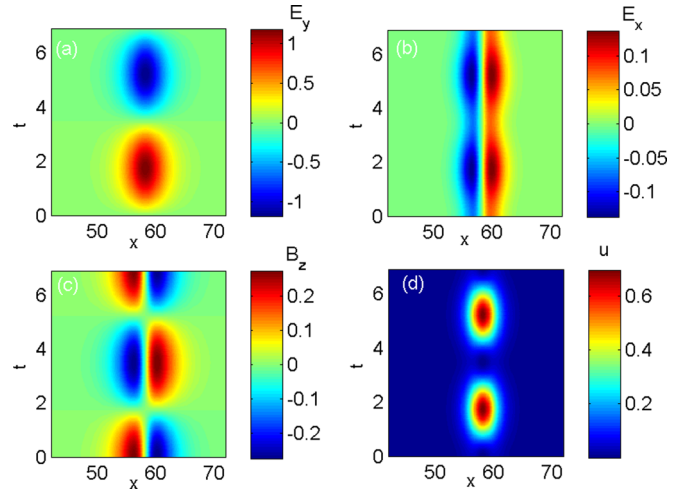
they have not been investigated by looking for exact solutions of the fluid model (as was done in this work for 1D waves and in Ref. [13] for 2D waves).

The maps in Figs. 3 and 6, depicting the spatial structure of the wave at a certain instant, suggest the existence of localized, time-periodic structures for which all plasma and electromagnetic perturbations vanish as $X \to \pm\infty$. However, we note that in our numerical solutions small-amplitude, periodic (standing wave) oscillations of the plasma and field variables exist at the tails of a linearly polarized solitary wave. This is shown in Fig. 7, which displays the spatial structure of the tail of the wave at a certain instant and the temporal structure at a certain position for $\Omega = 0.9\omega_{pe}$. Low-amplitude oscillations, of order 5×10^{-5}, in the vector potential are evident in the solitary wave's tails. These small-amplitude oscillations are connected to the periodic boundary conditions in our numerical formulation, since they can be thought of as corresponding to an interference pattern between outgoing waves which reenter the computational box from both sides.
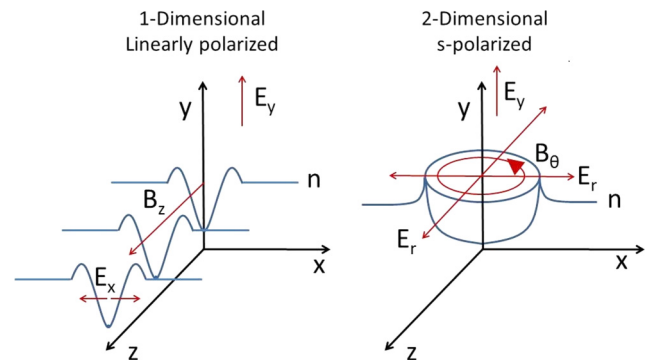

FIG. 5. (Color online) Schematics of the electron plasma density and the electromagnetic fields of 1D and 2D solitary waves with linear polarization $\boldsymbol{A} = A_y \boldsymbol{j}$.
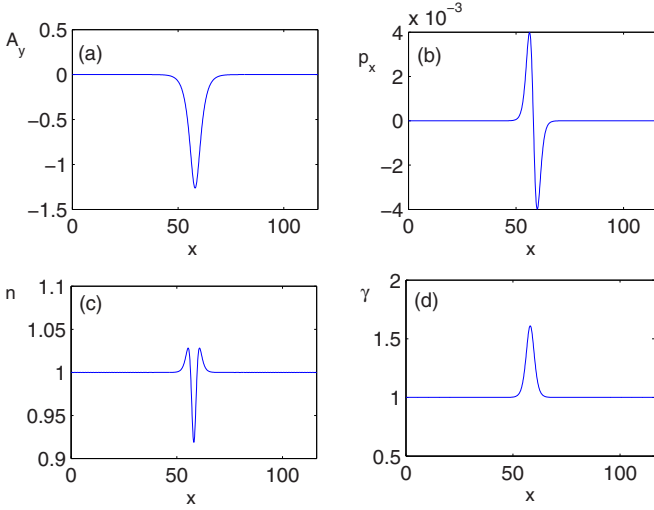
FIG. 6. (Color online) Spatial structure of a linearly polarized soliton with $\Omega = 0.9\omega_{pe}$ at a certain instant. Panels (a) to (d) show A_y, p_x, n, and γ, respectively.

We have found that, at a given frequency, the precise amplitude of the small oscillations depends on the initial guess, domain length and resolution of our Newton method, while at the same time the localized solitary wave structure remained the same. In particular, we have found oscillation amplitudes in the range 10^{-5}–10^{-2}, with no indication for a dependence of the amplitude on Ω. This indicates that, while the amplitude and profile of (the localized part of) the solitary wave are uniquely determined by Ω, there exists a continuum of solutions corresponding to tail oscillations of different amplitude.

Nevertheless, the standing wave oscillations in the tail are not completely arbitrary, but actually obey the dispersion relation of the Akhiezer-Polovin system, which is a particular case of Sys. (8). In the soliton's tail A_y and ϕ are very
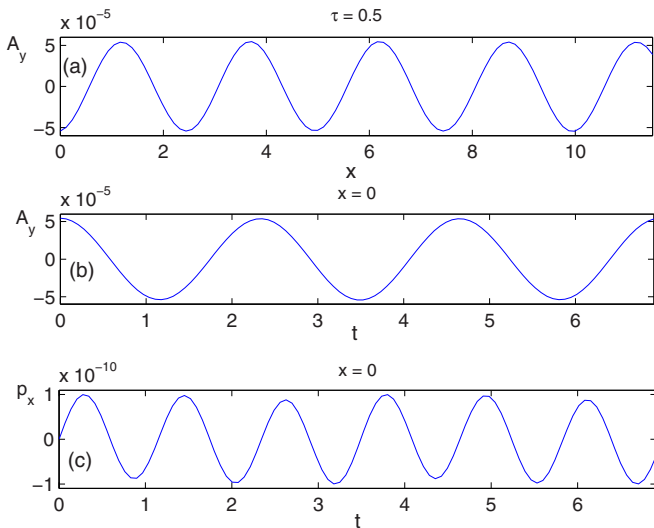

FIG. 7. (Color online) Vector potential at the tail of a solitary wave with $\Omega = 0.9\omega_{pe}$. Panel (a) shows the spatial structure at $\tau = 0.5$ and panel (b) the temporal behavior at $x = 0$.

small, thus indicating that the dynamics occurs close to the Akhiezer-Polovin equilibrium point $Q_0 \equiv (a, \dot{a}, \phi, \dot{\phi}) = (0,0,0,0)$. Around this equilibrium point oscillations following the dispersion relation given by Eq. (7) may occur. This statement is confirmed by looking closer to the small oscillations in the tail of a wave for the particular case of Fig. 7. From panels (a) and (b), which show the spatial structure at $\tau = 0.5$ and the temporal behavior at $x = 0$ of the vector potential, we find the frequency $\omega \approx 2.67\omega_{pe}$, the wave number $k \approx 2.51c/\omega_{pe}$, and $a_0 \approx 5 \times 10^{-5}$. Using $k = 2.51c/\omega_{pe}$ in Eq. (7) yields $\omega \approx 2.71\omega_{pe}$, which is in good agreement with $\omega \approx 2.67\omega_{pe}$. As expected, the longitudinal variable p_x has an amplitude of the order of $\sim a_0^2$ and oscillates with frequency 2ω [see panel (c)]. This argument also indicates why the amplitude of the tail oscillations is not uniquely determined: standing wave solutions satisfying Eq. (7) may be found for any (sufficiently small) a_0. For this reason, we consider the solitary waves presented here as localized structures.

C. Energy balance

Linearly polarized solitary waves are localized structures where electromagnetic energy and electron kinetic energy are exchanged periodically. This is an important difference compared to the circularly polarized waves, which exhibit a stationary character. Energy evolution is here analyzed using Eqs. (2a)–(2e). It conserves the sum of the three normalized energies, $E = E_l + E_p + E_e$, where

$$E_l = \frac{1}{2} \int \left[\left(\frac{\partial A_y}{\partial t} \right)^2 + \left(\frac{\partial A_y}{\partial x} \right)^2 \right] dx, \qquad (12)$$

$$E_p = \frac{1}{2} \int \left(\frac{\partial \phi}{\partial x} \right)^2 dx, \qquad (13)$$

$$E_e = \int (\gamma - 1) n \, dx. \qquad (14)$$

Here E_l, E_p, and E_e are the energy of the electromagnetic wave, the energy of the electrostatic plasma wave, and the kinetic energy of the electrons, respectively.

As observed in Ref. [22], linearly polarized breather-like solitary waves exhibit a periodic exchange of energy. This feature is shown in Fig. 8, which displays the time evolution of the three energy contributions for a solitary wave with $\Omega = 0.8\omega_{pe}$. In each period, the energy exchange is repeated twice; the two minimums in the electron kinetic energy coincide with the two maxima in the electromagnetic and plasma wave energies. The electrostatic energy, albeit being the smallest contribution, never vanishes, thus helping to maintain the plasma cavity.

IV. DIRECT NUMERICAL SIMULATION OF THE SOLITARY WAVES

Having discussed a new family of breather-like solitary wave solutions in the previous section, we now turn to direct fluid-Maxwell simulations of solitary waves of this family, in order to validate the numerical procedure that we used to detect these solutions. Moreover, since we integrate the
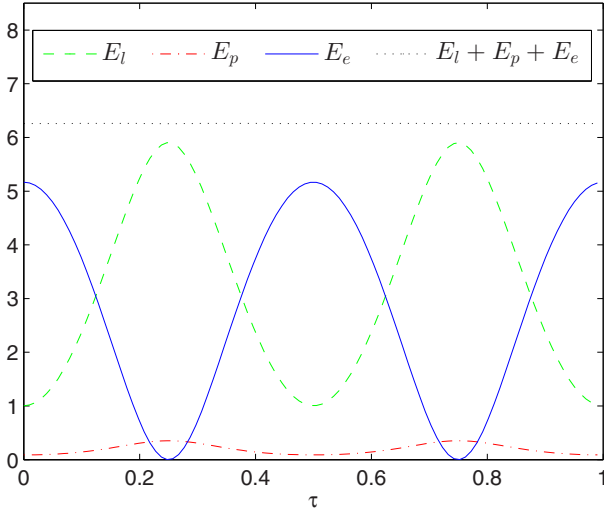
FIG. 8. (Color online) Evolution of the energy of the electromagnetic wave (E_l), the energy of the electrostatic plasma wave (E_p), and the kinetic energy of the electrons (E_e) for a solitary wave with frequency $\Omega = 0.8\omega_{pe}$. The black line represents the sum of the three terms.

FIG. 9. (Color online) Normalized variables of a Fluid-Maxwell simulation initialized with a solitary wave of frequency $\Omega = 0.75\omega_{pe}$.

fluid-Maxwell equations for several periods of the solitary wave, we expect that if these waves are prone to instabilities, these will be triggered within the simulation time. A more rigorous stability study is beyond the scope of this work. The simulations involve numerically solving the full relativistic fluid-Maxwell model [Eqs. (2a)–(2e)]. We have used two different codes for this purpose, a finite difference code and a pseudospectral one.

As all the time evolution equations we wish to solve here are either in continuity or convective form, it was very convenient to employ the subroutine package LCPFCT for the finite difference solver. LCPFCT is a freely available subroutine package developed at Naval Research Laboratory (NRL), USA [28]. These subroutines are based on the principle of flux-corrected transport [29]. Periodic boundary conditions are implemented for the simulations presented here, and Courant stability condition is used to calculate appropriate value of integration time step for ensuring the numerical stability. Profiles of fluid variables are specified at the grid centers, whereas the interface values of flow variables are used. The flux-correction method has been quite successful in solving fluid flow problems, and it ensures density positivity as well as numerical accuracy.

The pseudospectral code has been presented in Ref. [30] and uses Fourier space discretization of the partial derivative with respect to space and an adaptive, fourth order Runge-Kutta scheme for time stepping.

The initial conditions for the numerical simulations are chosen in accordance with the numerical solutions of Sec. III and are then evolved with above discussed method. In order to explore the full branch presented in Fig. 2, we ran several simulations. Each one was initialized with a solitary wave of a given frequency. For instance, Fig. 9 shows a fluid-Maxwell simulation initialized with a solitary wave of frequency $\Omega = 0.75\omega_p$, which is the one with highest amplitude that we simulated. In all cases the structures remain unchanged for
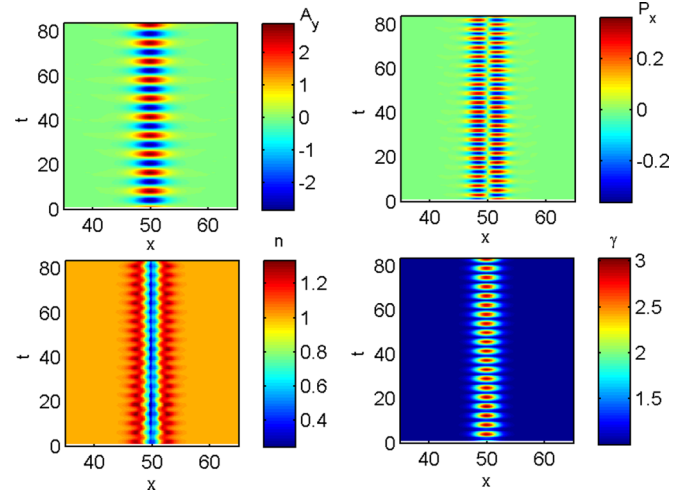
several plasma periods, and they do not seem to be prone to any instability. The amplitude and the oscillation frequency of the waves during the simulations coincide with the values expected from the analysis of Sec. III. The same is true for the frequency and wave number of the small oscillations in the tail. This confirms the integrity of the methodology and correctness of the solutions presented in this work. As the solitary waves appear stable, they are ideal candidates for further research, for example, for the investigation of the mutual collisions among two or more standing structures as has been studied for the circular polarization case in Refs. [30,31].

V. CONCLUSIONS

We have presented novel exact numerical solutions of the relativistic Maxwell-fluid model in a cold plasma with fixed ions. One-dimensional solitary waves with linear polarization and a breather-like behavior were computed by using a numerical method based on a finite-difference scheme. The spatiotemporal structure of the electromagnetic and plasma fields was presented as well as the main properties of the waves as a function of their frequency Ω. The solitary waves exist in the frequency range $\Omega_{\min} \equiv 0.694 < \Omega/\omega_{pe} < 1$, with $\Omega_{\min}$ the frequency value where the minimum of the plasma density vanishes. An analysis based on the different energy contributions showed that these localized structures consist of a plasma cavity where a periodic exchange of energy at frequency 2Ω occurs between an electromagnetic wave and the plasma electrons.

Unlike circularly polarized waves, which are stationary, linearly polarized waves exhibit a breather-like behavior. Longitudinal variables, like the electron momentum, oscillate with the frequency 2Ω; electrons are moved inward and outward from the plasma cavity twice per period. Besides this fundamental difference, other features of the solitary waves are shared by both types of polarization. For instance, the amplitude vanishes (is enhanced) and the width increases (decreases) as the frequency approaches to ω_{pe} ($\Omega_{\min}$). For a given frequency, the amplitude of linearly polarized waves

is greater than for circular polarization. The frequency range of existence is also broader.

It is well known that at the ion time scale solitons evolve to states called postsolitons. These are slowly expanding cavities in the ion and electron densities which trap electromagnetic energy and produce fast ions [9,32]. However, neglecting ion motion in our analysis is justified *a posteriori*, since the typical response time of the ions $(m_i/m_e)^{1/2} 2\pi /\omega_{pe}$, where m_i the ion mass, will be much larger than the typical period of oscillation $2\pi/\Omega$ for the solutions presented here.

In previous fluid [22] and PIC [23] simulations solitary-wave-like structures were excited by a linearly polarized high-intensity laser pulse incident on a plasma slab. However, since the waves were excited spontaneously during the complex interaction, this method has difficulties in providing important information like the amplitude-frequency dispersion relation or the frequency domain of existence. In addition, it is not clear if the excited solutions in these studies correspond to exact solitary waves. From this point of view, the procedure followed in this work is advantageous, complements the information of the simulations, and opens new possibilities. For instance, our fluid simulations, initialized with a single solitary wave, reveal that these coherent structures persist for a long time and give insight into the stability problem.

Since part of the electromagnetic energy is trapped inside the wave cavity, the solitary waves may play an important role in several applications like fast ignition in inertial confinement fusion. Past simulations, experiments, and theoretical work indicate that they are excited behind the laser pulse, and they seem to be a fundamental component of the laser-plasma interaction at high intensities. A good understanding of some aspects, like the excitation process or solitary wave interactions, are relevant for these applications. These scenarios can be analyzed by preparing fluid or particle-in-cell codes initialized with the solutions here presented. An example of this technique applied to relativistic solitons was given in Ref. [33], where stability, collisions, electromagnetic bursts, and postsoliton evolution of *s*-polarized 2D solitary waves were analyzed.

The present analysis can be extended to find moving solitary waves solutions with linear polarization in the relativistic fluid model. The small-amplitude limit of such solutions was presented in Ref. [10], thus suggesting that large-amplitude waves may also exist. The results of this work, which would complete our knowledge on the organization of linearly polarized solitary waves, will be presented elsewhere.

ACKNOWLEDGMENT

[1] S. Eliezer and K. Mima, *Applications of Laser-Plasma Interactions*, Series in Plasma Physics (Taylor & Francis, Philadelphia, 2008).

[2] A. Akhiezer and R. Polovin, Sov. Phys. JETP **3**, 696 (1956).

[3] V. A. Kozlov, A. G. Litvak, and E. V. Suvorov, Soviet Phys. JETP **49**, 75 (1979).

[4] P. K. Kaw, A. Sen, and T. Katsouleas, Phys. Rev. Lett. **68**, 3172 (1992).

[5] T. Z. Esirkepov, F. F. Kamenets, S. V. Bulanov, and N. M. Naumova, JETP Lett. **68**, 36 (1998).

[6] D. Farina and S. V. Bulanov, Phys. Rev. Lett. **86**, 5289 (2001).

[7] D. Farina and S. V. Bulanov, Plasma Phys. Controlled Fusion **47**, A260000 (2005).

[8] G. Sanchez-Arriaga, E. Siminos, and E. Lefebvre, Phys. Plasmas **18**, 082304 (2011).

[9] G. Sánchez-Arriaga, E. Siminos, and E. Lefebvre, Plasma Phys. Controlled Fusion **53**, 045011 (2011).

[10] L. Hadžievski, M. S. Jovanović, M. M. Škorić, and K. Mima, Phys. Plasmas **9**, 2569 (2002).

[11] A. Mancic, L. Hadžievski, and M. M. Škorić, Phys. Plasmas **13**, 052309 (2006).

[12] V. Saxena, A. Sen, and P. Kaw, Phys. Rev. E **80**, 016406 (2009).

[13] G. Sánchez-Arriaga and E. Lefebvre, Phys. Rev. E **84**, 036403 (2011).

[14] S. V. Bulanov, I. N. Inovenkov, V. I. Kirsanov, N. M. Naumova, and A. S. Sakharov, Phys. Fluids B **4**, 1935 (1992).

[15] S. V. Bulanov, T. Z. Esirkepov, N. M. Naumova, F. Pegoraro, and V. A. Vshivkov, Phys. Rev. Lett. **82**, 3440 (1999).

[16] T. Esirkepov, K. Nishihara, S. V. Bulanov, and F. Pegoraro, Phys. Rev. Lett. **89**, 275002 (2002).

[17] M. Borghesi, S. Bulanov, D. H. Campbell, R. J. Clarke, T. Z. Esirkepov, M. Galimberti, L. A. Gizzi, A. J. MacKinnon, N. M. Naumova, F. Pegoraro, H. Ruhl, A. Schiavi, and O. Willi, Phys. Rev. Lett. **88**, 135002 (2002).

[18] L. M. Chen, H. Kotaki, K. Nakajima, J. Koga, S. V. Bulanov, T. Tajima, Y. Q. Gu, H. S. Peng, X. X. Wang, T. S. Wen, H. J. Liu, C. Y. Jiao, C. G. Zhang, X. J. Huang, Y. Guo, K. N. Zhou, J. F. Hua, W. M. An, C. X. Tang, and Y. Z. Lin, Phys. Plasmas **14**, 040703 (2007).

[19] A. S. Pirozhkov, J. Ma, M. Kando, T. Z. Esirkepov, Y. Fukuda, L.-M. Chen, I. Daito, K. Ogura, T. Homma, Y. Hayashi, H. Kotaki, A. Sagisaka, M. Mori, J. K. Koga, T. Kawachi, H. Daido, S. V. Bulanov, T. Kimura, Y. Kato, and T. Tajima, Phys. Plasmas **14**, 123106 (2007).

[20] G. Sarri, D. K. Singh, J. R. Davies, F. Fiuza, K. L. Lancaster, E. L. Clark, S. Hassan, J. Jiang, N. Kageiwa, N. Lopes, A. Rehman, C. Russo, R. H. H. Scott, T. Tanimoto, Z. Najmudin, K. A. Tanaka, M. Tatarakis, M. Borghesi, and P. A. Norreys, Phys. Rev. Lett. **105**, 175007 (2010).

[21] F. Sylla, A. Flacco, S. Kahaly, M. Veltcheva, A. Lifschitz, G. Sanchez-Arriaga, E. Lefebvre, and V. Malka, Phys. Rev. Lett. **108**, 115003 (2012).

[22] D. Wu, C. Y. Zheng, X. Q. Yan, M. Y. Yu, and X. T. He, Phys. Plasmas **20**, 033101 (2013).

[23] A. Macchi, A. S. Nindrayog, and F. Pegoraro, Phys. Rev. E **85**, 046402 (2012).

[24] S. Poornakala, A. Das, P. K. Kaw, A. Sen, Z. M. Sheng, Y. Sentoku, K. Mima, and K. Nishikawa, Phys. Plasmas **9**, 3802 (2002).

[25] G. Lehmann and K. H. Spatschek, Phys. Rev. E **83**, 036401 (2011).

[26] T. C. Pesch and H.-J. Kull, Phys. Plasmas **14**, 083103 (2007).

[27] A. Champneys, Physica D **112**, 158 (1998).

[28] J. P. Boris, A. M. Landsberg, E. S. Oran, and J. H. Gardner, Tech. Rep. NRL/MR/6410–93-7192 (1993).

[29] J. P. Boris and D. L. Book, in *Controlled Fusion*, edited by J. Killeen (Academic Press, New York, 1976), pp. 85–129.

[30] E. Siminos, G. Sánchez-Arriaga, V. Saxena, and I. Kourakis, Phys. Rev. E **90**, 063104 (2014).

[31] V. Saxena, I. Kourakis, G. Sánchez-Arriaga, and E. Siminos, Phys. Lett. A **377**, 473 (2013).

[32] N. M. Naumova, S. V. Bulanov, T. Z. Esirkepov, D. Farina, K. Nishihara, F. Pegoraro, H. Ruhl, and A. S. Sakharov, Phys. Rev. Lett. **87**, 185004 (2001).

[33] G. Sánchez-Arriaga and E. Lefebvre, Phys. Rev. E **84**, 036404 (2011).